




# Dispersion model for level control of bubbling fluidized beds with particle cross-flow

Stefan Thanheiser<sup>1,\*</sup> , Markus Haider<sup>2</sup>

Institute for Energy Systems and Thermodynamics, TU Wien, Getreidemarkt 9/E302, Wien 1060, Austria

## ARTICLE INFO

### Keywords:

Bed level gradient  
Lateral mixing  
Horizontal mixing  
Air cushion  
Fictional density

## ABSTRACT

A fluidized bed with a large, continuous horizontal flow of particles (cross-flow) can lead to a sloped bed level, leaving a heat exchanger immersed in the fluidized bed covered by different amounts of particles. This facilitates particles bypassing the heat exchanger, thereby reducing its efficiency. Pressurized zones can be utilized to control the bed level along the particles' horizontal path, achieving a more even distribution of particles across the heat exchanger. Designing this level control system requires a physical model of the particle flow that accounts for the impact of pressurized zones, for which a new particle dispersion model was developed in this study. Dynamic simulations and experiments on a test rig were used to calibrate and validate the new particle dispersion model. The model was able to correctly predict the dynamic behavior of bed levels influenced by pressurized zones within a few millimeters. This model can be used to design and analyze a fluidized bed level control system. Further research on additional influencing factors of particle dispersion, in particular the heat exchanger's configuration, is still required to achieve general applicability of the new particle dispersion model.

## 1. Introduction

### 1.1. Background

When particles are continuously added to one side of a fluidized bed with a rectangular cross-section, they slowly travel to the other side. This horizontal movement of particles super-positioned with their regular vertical movement within fluidized beds is called a *cross-flow*<sup>3</sup> (Sette et al., 2015; p. 245) and has many applications, such as drying (Daud, 2008; p. 407), indirect gasification (Sette et al., 2015; p. 245), and particle receivers in both concentrating solar power (CSP) (Gómez-Hernández et al., 2018) and solar calcination (Esence et al., 2020) systems.

The present study focused on thermal energy storage (TES) applications, in which a heat exchanger immersed in the fluidized bed is used to add and extract thermal energy to and from the particles, which act as the storage material (Steiner et al., 2016; p. 3). Such fluidized bed heat exchangers (FBHEs) employ fluidization velocities that are only slightly above incipient fluidization to maximize the surface-to-bed heat transfer coefficient while minimizing heat losses and the energy required for

fluidization (Salatino et al., 2016; p. 98). At such low fluidization velocities, adding large amounts of particles to a long bed can result in a visible slope of the bed level along the particles' horizontal path (Schwaiger, 2016; p. 86). However, a sloped bed level means that the heat exchanger in the fluidized bed is covered by different amounts of particles, as pictured in Fig. 1.

Since the heat exchanger poses an impediment to the particle cross-flow (Eder et al., 2021; p. 7426), a large portion of the particles flow over the heat exchanger instead of passing through it. This bypass limits the heat exchanger's ability to add and extract thermal energy to and from the particles. Schwaiger (2016; pp. 89–91) proposed pressurized zones, called *air cushions*, to even out the bed levels along the particles' path and limit the number of particles bypassing the heat exchanger, as depicted in Fig. 1b. Each air cushion creates a pressurized chamber by collecting the fluidization gas and continuously releasing it again through valves. Each valve controls the pressure in its respective chamber in such a way that the fluidized bed is pushed down and the bed level is closer to the heat exchanger.

\* Corresponding author.

E-mail addresses: [stefan.thanheiser@tuwien.ac.at](mailto:stefan.thanheiser@tuwien.ac.at) (S. Thanheiser), [markus.haider@tuwien.ac.at](mailto:markus.haider@tuwien.ac.at) (M. Haider).

<sup>1</sup> <https://orcid.org/0000-0003-2765-1156>

<sup>2</sup> <https://orcid.org/0000-0002-0054-4206>

<sup>3</sup> Other authors write *crossflow* (Kunii and Levenspiel, 1991a; p. 338)

**Nomenclatures***Abbreviation*

CCBM	Counter-current backmixing model
CSP	Concentrating solar power
DoE	Design of experiments
FBHE	Fluidized bed heat exchanger
HTF	Heat transfer fluid
PDF	Probability distribution function
PDM	Particle dispersion model
PI	Proportional-Integral
PLC	Programmable logic controller
TES	Thermal energy storage

*Symbol*

$A$	Cross-section area, $m^2$
$Ar$	Archimedes number, -
$B, a, b, c$	Constants or exponents, -
$C$	Controller transfer function, -
$D$	Dispersion or diffusion coefficient, $m^2/s$
$d$	Diameter, m
$e$	Control error, m
$g$	Gravitational acceleration, $m/s^2$
$h$	Bed height, m
$K_p$	Proportional gain, $1/m$
$L$	Bed width, m
$m$	Particle mass, kg
$\dot{m}$	(Particle) mass flow, $kg/s$
$P$	Plant transfer function, -
$p$	Pressure, Pa
$p_\chi$	Chi-square level of significance, -
$S$	Source or sink, $kg/(m^3s)$

$T$	Temperature, K
$T_i$	Integration time, s
$t$	Time, s
$w$	Velocity, m/s
$X$	Measured bed level, m
$x$	Length (horizontal), m
$Y$	Valve actuating value, -
$\Delta$	Difference operator, -
$\varepsilon$	Mean bed voidage or exponent, -
$\lambda$	Distance, m
$\mu$	Dynamic viscosity (Pa s) or expected value (m)
$\pi$	Dimensionless variable, -
$\rho$	Density, $kg/m^3$
$\Phi$	Fictional density, $kg/m^3$
$\varphi_s$	Particle sphericity, -

*Subscripts*

A	Fluidization air
AC	Air cushion
Ar	Archimedes
bed	Fluidized bed
e	Excess
g	Fluidization gas
left, center, right	Positions in the bed
mf	Minimum fluidization
p	Particle
ref	Reference
S	Specific
tubes	Covered by tubes
weir	Outlet weir
0	Free or empty

**1.2. Research problem and gap**

However, thus far, the air cushion concept has only been described empirically, such as by [Schwaiger \(2016; pp. 89–91\)](#) and [Steiner et al. \(2016; pp. 4–5\)](#), but no actual control system has been designed, tested, or published. Any proper design of a control system requires a mathematical model of the physical processes involved ([Keviczky et al., 2019a; p. 24](#)), meaning a model able to describe the relationship between the

cross-flow of particles and the resulting bed level and how the bed level is affected by the air cushions. Although previous research has studied horizontal mixing and dispersion of particles in fluidized beds in great detail, the influence of sloped bed levels or pressurized zones on a cross-flow of particles has largely been neglected.

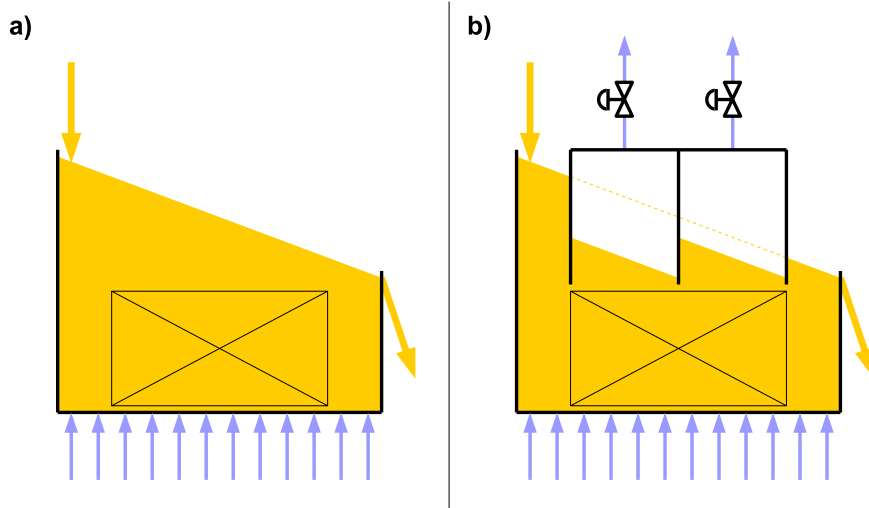


**Fig. 1.** Sloped bed level along a fluidized bed heat exchanger a) without, b) with the use of pressurized zones to control the bed level. The orange area represents the fluidized bed. Orange arrows represent particle flow. Blue arrows show flow of fluidization gas. The heat exchanger is represented by a crossed-out box.

### 1.3. Research objectives

This study aims to bridge the research gap identified above and develop a new particle dispersion model (PDM) that can accurately describe the processes involved in an air cushion control system. Furthermore, the new PDM is tested (validated) to ascertain if it is fit for purpose.

### 1.4. Outline

Section 2 includes the literature review. The development of the new PDM is described in detail in Section 3. Section 4 then describes the methods used to calibrate and test (validate) the new PDM and the results are reported in Section 5.

Collected data for this work is available in the data repository (Thanheiser and Haider, 2025); software can be found in the software repository (Thanheiser, 2025).

## 2. Literature review

The literature review presented here served to inform the development of the new PDM. This section therefore discusses previous work on particle dispersion related to the conditions investigated in this study: fluidized beds operated at low fluidization velocities with particle cross-flow that include a heat exchanger and sections separated by baffles.

The horizontal movement of particles in fluidized beds is generally described as *horizontal* (Kunii and Levenspiel, 1991a; p. 211) or *lateral mixing* (Sette et al., 2014; p. 74). The mechanisms of horizontal mixing are closely related to bubbles (Kunii and Levenspiel, 1991a; pp. 219–223), which affect mixing on two different scales: a smaller scale of individual bubbles and a larger scale of gross particle circulation induced by preferential bubble paths (Kunii and Levenspiel, 1991a; p. 211).

### 2.1. Horizontal mixing – small scale

Individual bubbles rising through the fluidized bed affect horizontal mixing in the following ways:

- Bubbles bursting at the surface throw particles into the open space above (the freeboard) (Kunii and Levenspiel, 1991b; p. 167). Particles that are not elutriated out of the freeboard by the fluidization gas fall back down to the bed, scattering across an area around the bubble and contributing to their horizontal displacement (Santana et al., 2005; p. 4).
- Bubbles collect particles close to them in their wake on their way up the bed. Particles mix in the wake and randomly leave it again at a different horizontal position than before (Kunii and Levenspiel, 1969).
- Downward drifting particles replacing those that were transported upwards in a bubble's wake must also move laterally under the bubble's path. This mechanism is also described by the counter-current backmixing model (CCBM) (Abanades and Grasa, 2001; p. 5658).

### 2.2. Horizontal mixing – large scale

On a larger scale, bubbles tend to flow in preferential paths depending on the bed's dimensions (deep or shallow) and its gas distributor, leading to different particle circulation patterns (Kunii and Levenspiel, 1991c; p. 140). Toroidal circulation structures may form in long shallow beds (Pallarès et al., 2007; p. 934) called *mixing cells* (Sette et al., 2014; p. 75). If tuyeres are used in the gas distributor, mixing cells form around the chain of bubbles created by the nozzles; thus, the number of nozzles defines the number and size of mixing cells (Olsson et al., 2012; p. 152). Without nozzles, mixing cells are about as large as

the smallest dimension of the fluidized bed, which is its height in the case of shallow beds and its width or diameter in the case of deep beds (Subbarao et al., 1985; p. 1988). Particles changing mixing cells, either by being thrown by a bursting bubble into a different cell or by switching to an adjacent downward drift, account for the net horizontal transport of particles across the entire bed (Olsson et al., 2012; pp. 150–151).

### 2.3. Impact of immersed heat exchangers

Adding a densely packed tube bank to a fluidized bed does not substantially change the gross circulation pattern of the particles, but it slows down the average axial particle velocity by approximately 90 % (Chen et al., 1983; pp. 206–210). Tube banks also promote splitting and coalescence of bubbles (Asegehegn et al., 2011a; p. 5425), resulting in a smaller average bubble size and a more uniform distribution of fluidization gas (Li et al., 2011; p. 6224). Bubble size inside the tube bank is largely independent of the fluidization gas flow and the distance from the distributor floor, and it is mostly controlled by the tube bank's geometry (Asegehegn et al., 2011b; p. 258). Recent numerical simulations support these findings (Li et al., 2011; pp. 6224–6226; Kuipers et al., 1992; p. 199).

### 2.4. Impact of particle cross-flow and baffles

Particle cross-flow can suppress the formation of clearly defined mixing cells by blurring preferential bubble paths (Sette et al., 2016; pp. 308–309). Martínez Castilla et al. (2020; pp. 98, 100–101) found that introducing a baffle slightly above the level of a shallow (0.11 m) bed to block the particle splash reduced horizontal mixing in the baffle's vicinity by about 90 %.

### 2.5. Modeling horizontal mixing

Horizontal mixing is usually modeled as dispersion with a diffusion equation describing the flow of particles (Olsson et al., 2012; p. 149):

$$\frac{\partial C}{\partial t} = \frac{\partial}{\partial x} \left( D \frac{\partial C}{\partial x} \right) \quad (1)$$

$C$  is the concentration of a tracer or fuel particle,  $t$  is time,  $x$  is the direction in which the concentration  $C$  changes, and  $D$  is the dispersion coefficient. This transport equation is a non-stationary, one-dimensional diffusion equation for a closed system. Using a diffusion equation to model particle dispersion typically implies a homogeneous fluidized bed or a fluidized bed that is much larger than the characteristic mixing length scale, which is identical to the size of a mixing cell (Olsson et al., 2012; p. 150).

To include particle cross-flow in the transport equation above, one approach is to use an “average” particle dispersion coefficient  $D$  that combines both regular particle dispersion and the impact of the convective cross-flow (Olsson et al., 2012; p. 149). Some authors, such as Sette et al. (2015; p. 247) and Shi and Fan (1985; p. 24), have chosen to add a convective term to the transport equation to describe the particle cross-flow and have the dispersive term only describe regular particle dispersion without a cross-flow.

Differential equations describing a continuous flow of particles in and out of a fluidized bed have fundamentally different boundary conditions than those describing batch processes or Brownian motion in a closed system (Shi and Fan, 1985; p. 24). Dispersion models for batch processes include, for example, Bellgardt and Werther (1986; p. 174), Kunii and Levenspiel (1991a; pp. 220–222), and Shi and Fan (1984; p. 338).

### 2.6. Driving force of particle dispersion

As in Eq. 1, the gradient of a concentration of sparsely distributed

tracer or fuel particles  $\partial C/\partial x$  is typically the driving force of particle dispersion, as seen in the models by Pallarès et al. (2007; pp. 932–933) and Olsson et al. (2012; p. 152). Alternatively, Sette et al. (2015; p. 247) introduced a dispersion model where the gradient of a fictional bed material density  $\partial\Phi/\partial x$  is the driving force of dispersion:

$$0 = \frac{\partial}{\partial x} \left( D \frac{\partial\Phi}{\partial x} \right) + S \quad (2)$$

where  $S$  is a sink or source term for bed material. Sette et al. did not make it entirely clear how the fictional bed density  $\Phi$  was defined. They used Eq. 2 and potential flow theory to derive the stationary velocity field of a bed material cross-flow to describe how the cross-flow of bulk solids influenced the dispersion of sparsely distributed fuel particles (Sette et al., 2015; pp. 247, 251).

Schwaiger (2016; p. 86) suggested that different bed levels create a horizontal pressure gradient and that this pressure gradient pushes the particles from the side with a higher bed level to the one with a lower bed level, thus creating a horizontal movement of particles. He did not include this theory in any sort of dispersion model.

## 2.7. Particle dispersion coefficients

One common way to quantify the particle dispersion coefficient  $D$  is the random walk theory for Brownian motion developed by Einstein (1905; p. 559):

$$D = \frac{\lambda^2}{2\Delta t} \quad (3)$$

where  $\Delta t$  is the mean time it takes a suspended molecule to travel the distance  $\lambda$ . The random walk theory forms the basis of many PDMs, such as Köhler et al. (2021; p. 6) and Liu and Chen (2010; pp. 2117–2119). In these models, the gradient of a concentration of tracer or fuel particles  $\partial C/\partial x$  is the driving force of dispersion.

Alternatively, Shi and Fan (1984; pp. 339–340) identified three main modes of horizontal mixing, namely bubble movement, bursting bubbles, and gross circulations, and derived their influencing factors: excess fluidization velocity  $w_e$ , which is the difference between the superficial velocity and the minimum fluidization velocity  $w - w_{mf}$ ; Kunii and Levenspiel (1991c; p. 137); bed height at minimum fluidization conditions  $h_{mf}$ ; particle diameter  $d_p$ ; fluidization gas density  $\rho_g$ ; the difference between particle and fluidization gas density  $\rho_p - \rho_g$ ; and fluidization gas dynamic viscosity  $\mu_g$ . They then used dimensional analysis to obtain an equation of dimensionless factors that describes the particle dispersion coefficient  $D$ :

$$\frac{D}{(w - w_{mf})h_{mf}} = B \left( \frac{(w - w_{mf})d_p\rho_g}{\mu_g} \right)^a \left( \frac{h_{mf}}{d_p} \right)^b \left( \frac{\rho_p - \rho_g}{d_p} \right)^c \quad (4)$$

Experiments were performed to identify the remaining coefficients as  $B = 0.46$ ,  $a = -0.21$ ,  $b = 0.24$ , and  $c = -0.43$ .

## 2.8. Influencing factors of particle dispersion

Identifying the influencing factors of particle dispersion is a prerequisite for using dimensional analysis to find an equation for the particle dispersion coefficient (Szirtes, 2007). Most of the factors identified by Shi and Fan (1984; p. 339) listed above are included in either the Reynolds or Archimedes number that together describe the state of fluidization (Kunii and Levenspiel, 1991d; pp. 80, 89).

Bed height  $h_{mf}$  determines the size to which bubbles can grow, which impacts the horizontal mixing caused by bursting bubbles: deeper beds produce larger bubbles (Mori and Wen, 1975; pp. 109–110), which in turn create greater entrainment (Kunii and Levenspiel, 1991b; p. 168). This factor may also be used to account for the intensity of particle circulation (Oke et al., 2014; p. 122) or for the influence of a grid zone

near the distributor floor (Shi and Fan, 1985; p. 25).

In an extension of their original model including a continuous flow of particles, Shi and Fan identified the mean horizontal particle velocity  $w_p$  as an additional influencing factor of particle dispersion (Shi and Fan, 1985; p. 25).

Oke et al. (2014; pp. 119, 123–124) adapted Shi and Fan's approach and added the bed's width as an additional influencing factor, but it only had a significant impact on the dispersion coefficient in very narrow beds.

## 2.9. Conclusions

Much of the previous work on particle mixing in fluidized beds has focused on fuel particles in fluidized bed boilers (Sette et al., 2015, 2014; Pallarès et al., 2007; Olsson et al., 2012; Sette et al., 2016; Köhler et al., 2021; Liu and Chen, 2010; Farzaneh et al., 2013; Guío-Pérez et al., 2023; Salatino and Solimene, 2017; Lundberg et al., 2017). Compared to fluidized bed heat exchangers, fluidized bed boilers are typically shallow (Pallarès et al., 2007; p. 929), and they often do not contain tube banks. The flow of fluidization gas is determined by the stoichiometry of the incineration, whereas fluidized bed heat exchangers aim to optimize the surface-to-bed heat transfer coefficient at rather low fluidization gas flows (Salatino et al., 2016; p. 98).

Most PDMs use the gradient of a concentration of sparsely distributed fuel particles as the driving force of dispersion, which does not account for the impact of the bed level. Sette et al. (2015; p. 247) introduced a fictional density that may include the bed level but did not describe it in detail and used it for a purpose where bed levels were not of concern. Schwaiger (2016; p. 86) made several empirical observations on how the bed level impacts horizontal mixing but did not include it in a dispersion model. No dispersion model includes the impact of pressurized zones.

This leaves a research gap with respect to dispersion models suitable for the conditions investigated in this study that use the bed level gradient created by a large particle cross-flow as the driving force of dispersion and that include the impact of pressurized zones on the bed level. This gap is filled by developing a new PDM using several of the works discussed in this review:

- The inclusion of a densely packed tube bank severely slows down gross circulations (Chen et al., 1983; pp. 206–210) and distributes fluidization gas more evenly (Li et al., 2011; p. 6224). A particle cross-flow can further suppress the formation of mixing cells (Sette et al., 2016; pp. 308–309). Furthermore, models that include mixing cells, such as Olsson et al. (2012), are considered impractical for the purpose of describing a continuous control system for the bed level. It is therefore reasonable to assume a homogeneous fluidized bed without gross circulation structures such as mixing cells in the new PDM.
- The new PDM combines Schwaiger's empirical observation that the pressure gradient created by the bed level gradient is the driving force of dispersion (Schwaiger, 2016; p. 86) with the fictional density concept from Sette et al. (2015; p. 247) in Eq. 2. This results in a transport equation that (indirectly) uses a pressure gradient, created either by different bed levels or by pressurized zones, as the driving force of dispersion.
- The new PDM uses an average particle dispersion coefficient for both regular particle dispersion and the particle cross-flow, which is reasonable according to Olsson et al. (2012; p. 149). A convective term is therefore not included in the new PDM, simplifying it.
- The new PDM's omission of a convective term, its driving force of dispersion (a pressure gradient) as well as its boundary conditions (including particle cross-flow) make it unlikely that its dispersion coefficients are easily comparable to other sources in literature. Thus, following the approach by Shi and Fan (1984; pp. 339–340), dimensional analysis is used to develop an equation for the particle dispersion coefficient. The influencing factors of particle dispersion



identified by [Shi and Fan \(1984; p. 339\)](#), ([Shi and Fan, 1985; p. 25](#)) are reused. Very narrow beds are not considered relevant for fluidized bed heat exchangers; hence, the bed's width does not have a significant impact on particle dispersion ([Oke et al., 2014; pp. 123–124](#)) and is therefore not included as an influencing factor in the dimensional analysis.

- Baffles can severely reduce particle dispersion in their vicinity by blocking the particle splash ([Martinez Castilla et al., 2020; p. 101](#)). However, an air cushion control system only aims to control the bed level within individual chambers (between baffles), not across several chambers (across baffles). Hence, identifying the exact mode by which baffles influence the horizontal flow of particles is considered outside the scope of this study and not included in the new PDM.

### 3. Particle dispersion model

This section presents the new (proposed) PDM. [Section 3.1](#) derives the transport equation (the actual PDM) and [Section 3.2](#) conducts the dimensional analysis of the PDM's dispersion coefficient.

#### 3.1. Transport equation

When modeling horizontal particle dispersion as diffusion, the mass flow of particles is governed by Fick's law ([Ferziger et al., 2020; pp. 9–10](#)):

$$\dot{m}_s = -D \frac{\partial \Phi}{\partial x} \quad (5)$$

where  $\dot{m}_s$  is the mass flux per flow area in  $\text{kg}/(\text{m}^2\text{s})$ ,  $D$  is the diffusivity in  $\text{m}^2/\text{s}$ , and  $\partial \Phi / \partial x$  is the gradient of a concentration  $\Phi$  by the horizontal coordinate  $x$ . The concentration term  $\Phi$ , which has the unit  $\text{kg}/\text{m}^3$ , can be interpreted as the concentration of particle mass per an arbitrary control volume, that is, a *density*. This control volume has a fixed size and is not identical to the suspension's volume. Therefore,  $\Phi$  will be called a *fictional density* from this point on.

A greater bed level in one section of the fluidized bed is equal to a greater concentration of particle mass there and, hence, a greater fictional density  $\Phi$ . Different bed levels create different quasi-hydrostatic pressures in the bed, and this pressure gradient pushes the particles from the side with a greater bed level to the side where the bed level is lower ([Steiner et al., 2016; p. 4](#)). The connection between

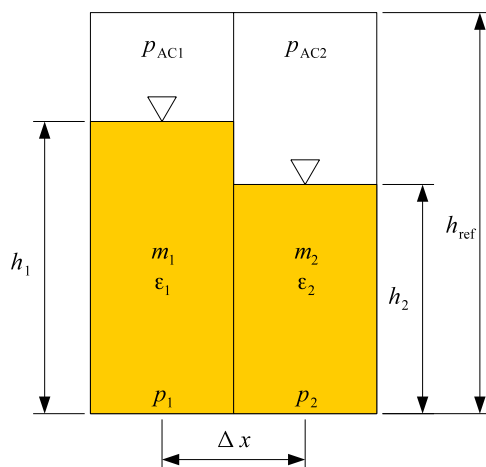


**Fig. 2.** Sketch to illustrate the connection between fictional density, bed level, and bed pressure. The two control volumes (indices  $i = 1$  and  $2$ ) each contain a mass of particles  $m_i$  (orange area) with a voidage  $\varepsilon_i$  at a bed level  $h_i$  with an air cushion pressure  $p_{ACi}$  above the bed level, creating a pressure  $p_i$  at the bed's floor. Each control volume has a reference height  $h_{ref}$  and a length of  $\Delta x$ .

fictional density, bed level, and bed pressure is demonstrated with the help of [Fig. 2](#).

[Fig. 2](#) shows two control volumes in a fluidized bed at different bed levels. The bed's fictional density  $\Phi_{bed1}$  is defined as the fraction of particle mass within the entire control volume 1 with height  $h_{ref}$ :

$$\Phi_{bed1} = \frac{m_1}{h_{ref}L\Delta x} \quad (6)$$

The term  $L$  describes the bed's width, which is assumed to be constant. The mass of particles  $m_1$  in the control volume 1 follows from [Fig. 2](#) as

$$m_1 = \rho_p(1 - \varepsilon_1)h_1L\Delta x \quad (7)$$

where  $\rho_p$  is the (raw) particle density and  $\varepsilon_1$  is the bed's mean voidage (volume fraction of gas). The bed voidage is not entirely uniform inside the fluidized bed:

- In the vertical direction, bed voidage is primarily a function of the fraction of the bed in bubbles ([Kunii and Levenspiel, 1991c; p. 155](#)), which is a function of the rise velocity of bubbles ([Kunii and Levenspiel, 1991c; pp. 156–157](#)), which in turn is a function of the bubble size ([Kunii and Levenspiel, 1991c; p. 147](#)). As mentioned in [Section 2](#), bubble size inside an immersed heat exchanger is near constant, thereby limiting variations in bed voidage in the vertical direction.
- In the horizontal direction, bed voidage can change due to different fluidization velocities. Different bed heights cause different back pressures on the fluidization gas distributor, which may result in greater fluidization and, therefore ([Kunii and Levenspiel, 1991c; pp. 156–157](#)), bed voidage where the bed height is lower. However, since the fictional density is defined by the mass of particles alone ([Eq. 6](#)), variations in the bed voidage in the horizontal direction are implicitly accounted for in this model.

For the kind of fluidized bed investigated in this study, which includes an immersed heat exchanger that is covered by only moderate amounts of particles (in particular when the bed level control system is active) and is only moderately fluidized, the bed voidage in the entire bed changes very little in either direction. Observations by the authors have shown that the bed voidage only increases by a few percentage points above the bed voidage at minimum fluidization conditions. For the purpose of this study, the bed voidage was therefore considered near constant.

Substituting  $m_1$  in [Eq. 6](#) with [Eq. 7](#) yields the fictional bed density  $\Phi_{bed1}$  as a function of the (actual) bed level  $h_1$ :

$$\Phi_{bed1} = \rho_p(1 - \varepsilon_1) \frac{h_1}{h_{ref}} \quad (8)$$

Hence, the fictional bed density  $\Phi_{bed1}$  may be measured by measuring the bed level  $h_1$ .

The fictional bed density  $\Phi_{bed1}$  can be transformed into an equivalent bed pressure. For now, the air cushion pressures  $p_{AC}$  are omitted. The pressure  $p_1$  at the bottom of control volume 1 is then defined as ([Kunii and Levenspiel, 1991d; p. 69](#))

$$p_1 = (\rho_p - \rho_g)(1 - \varepsilon_1)h_1g \quad (9)$$

where  $\rho_g$  is the fluidization gas density and  $g$  is the gravitational acceleration. The particle density is typically far larger than the gas density  $\rho_p \gg \rho_g$ . This was also the case in the test rig used in this work, which used quartz sand ( $\text{SiO}_2$ ) with a density  $\rho_p$  of about  $2650 \text{ kg}/\text{m}^3$  ([Greenwood and Earnshaw, 1997; p. 344](#)) as the bed material and dry air with a density  $\rho_g$  of less than  $1.1 \text{ kg}/\text{m}^3$  at operating conditions (bed temperature greater than  $50^\circ\text{C}$ ) ([Wagner et al., 2010; p. 173–174](#)) as the fluidization gas. Hence, [Eq. 9](#) can be simplified to

$$p_1 \approx \rho_p(1 - \varepsilon_1)h_1g \quad (10)$$

Combining Eqs. 8 and 10 yields

$$p_1 = \Phi_{\text{bed1}}h_{\text{ref}}g \quad (11)$$

Hence, the fictional density  $\Phi_{\text{bed1}}$  effectively condenses the bed's influencing factors on the pressure  $p_1$ , namely bed level, particle density, and voidage, into a single variable in conjunction with an (arbitrary) reference height  $h_{\text{ref}}$ . Using Eq. 11, the additional air cushion pressure above the bed level  $p_{\text{AC1}}$  can be turned into an additional fictional density  $\Phi_{\text{AC1}}$ :

$$\Phi_{\text{AC1}} = \frac{p_{\text{AC1}}}{h_{\text{ref}}g} \quad (12)$$

The sum of the fictional densities of the bed  $\Phi_{\text{bed1}}$  and the air cushion  $\Phi_{\text{AC1}}$  constitutes the (total) fictional density  $\Phi_1$ :

$$\Phi_1 = \Phi_{\text{bed1}} + \Phi_{\text{AC1}} \quad (13)$$

Thus, a change in the air cushion pressure  $p_{\text{AC1}}$  leads to an equivalent change in the total fictional density  $\Phi_1$ . Changing the air cushion pressure  $p_{\text{AC1}}$  also changes the pressure gradient between the two control volumes in Fig. 2, resulting in a movement of particles between them. Since the air cushion pressure and the fictional density are coupled via Eq. 12, this pressure gradient can be expressed as an equivalent gradient of the fictional density (see also Eq. 11):

$$\frac{\partial p}{\partial x} = \lim_{\Delta x \rightarrow 0} \left( \frac{p_2 - p_1}{\Delta x} \right) = \lim_{\Delta x \rightarrow 0} \left( \frac{\Phi_2 - \Phi_1}{\Delta x} h_{\text{ref}}g \right) = \frac{\partial \Phi}{\partial x} h_{\text{ref}}g \quad (14)$$

This equation demonstrates how bed pressure, particle mass, and fictional density are coupled across control volumes, making the fictional density  $\Phi$  a conserved quantity, for which a conservation equation can be written in Cartesian coordinates as (Ferziger et al., 2020; p. 11)

$$\frac{\partial \Phi}{\partial t} = \frac{\partial}{\partial x} \left( D \frac{\partial \Phi}{\partial x} \right) + S \quad (15)$$

where  $t$  denotes the time and  $S$  a source or sink of particles (adding or extracting particles to or from the bed). This transport equation is the mathematical form of the new (proposed) PDM and is identical to Eq. 2 by Sette et al. (2015; p. 247) but in a nonstationary form. This equation does not include any form of convection. The entire particle transport in the horizontal direction is modeled as dispersion.

Although the choice of reference height  $h_{\text{ref}}$  is arbitrary and can even be smaller than the actual bed levels occurring in the fluidized bed, it is recommended to set  $h_{\text{ref}} = 1$  m and interpret the fictional bed density  $\Phi_{\text{bed}}$  as the particle mass per floor area and unit bed height according to Eq. 6; this also makes the specific mass flow  $\dot{m}_s$  in Eq. 5 a more standardized measure, which is based on the reference height  $h_{\text{ref}}$  rather than the actual bed level:

$$\dot{m}_s = \frac{\dot{m}}{h_{\text{ref}}L} \quad (16)$$

This definition is a direct consequence of defining the fictional bed density  $\Phi_{\text{bed}}$  as the particle mass per control volume with constant height  $h_{\text{ref}}$  (see Eq. 6).

### 3.2. Dispersion coefficient

As mentioned in Section 2, based on Shi and Fan (1984; pp. 339–340), dimensional analysis in conjunction with experiments were used to determine an equation for the particle dispersion coefficient  $D$  contained in the proposed PDM in Eq. 15. The variables considered relevant influencing factors of particle dispersion are listed in Table 1.

This list is identical to the influencing factors suggested by Shi and Fan (1984; p. 339), (Shi and Fan, 1985; p. 25) with the following changes: the gravitational acceleration  $g$  is added to the list of variables,

**Table 1**

Relevant variables (influencing factors) for the dimensional analysis of particle dispersion.

Symbol	Description	Dimension
$D$	Particle dispersion coefficient	$\text{m}^2/\text{s}$
$w_e$	Excess fluidization velocity	$\text{m}/\text{s}$
$w_p$	Mean horizontal particle velocity	$\text{m}/\text{s}$
$(\rho_p - \rho_g)$	Difference between particle and gas density	$\text{kg}/\text{m}^3$
$\rho_g$	Fluidization gas density	$\text{kg}/\text{m}^3$
$\mu_g$	Fluidization gas dynamic viscosity	$\text{kg}/(\text{m}\cdot\text{s})$
$d_p$	Mean particle diameter	$\text{m}$
$g$	Gravitational acceleration	$\text{m}/\text{s}^2$

and the bed's height at minimum fluidization conditions  $h_{\text{mf}}$  is removed. The omission of the gravitational acceleration  $g$  appears to be a mishap in Shi and Fan's dimensional analysis since they clearly account for it in their model for bubble rise velocity and they attribute other influencing factors of particle dispersion to bubble rise velocity (Shi and Fan, 1984; p. 339). The bed height at minimum fluidization conditions  $h_{\text{mf}}$  is omitted for several reasons:

- As mentioned in Section 2, bed height does have an influence on particle dispersion by impacting the size to which bubbles can grow, particle circulation, and a possible grid-zone effect. However, neither the bed's height nor the configuration of the immersed tube bundle, which has similar effects as bed height (see Section 2), could be altered in a meaningful way in the test rig used in this work. Since their influence could not be measured, these factors are omitted from the proposed model.
- The only way to change the bed height in the test rig is by changing the flow of particles going through it. This, however, makes the bed height a function of the mean horizontal particle velocity  $w_p$ , and thus the influence of the particle flow on the bed height is already implicitly included in the use of  $w_p$  as an influencing factor.

Besides the mean particle diameter  $d_p$ , the particle sphericity  $\varphi_s$  as well as the bed voidage at minimum fluidization conditions  $\varepsilon_{\text{mf}}$  are implicitly included as influencing factors since they are influencing factors of the minimum fluidization velocity  $w_{\text{mf}}$  Kunii and Levenspiel (1991d; p. 69) and, thereby, the excess fluidization velocity  $w_e$ .

The chosen *dimensional set* (Szirtes, 2007; p. 164) is shown in Table 2.

The dimensionless variables (pi-factors) derived from Table 2 are listed in Eq. 17.

**Table 2**

Dimensional set. The table should be read as a matrix separated into submatrices: submatrix  $A$  (rows 1–3, columns 6–8), submatrix  $B$  (rows 1–3, columns 1–5), submatrix  $D = I$  (rows 4–8, columns 1–5), and submatrix  $C = -D(A^{-1}B)^T$  (rows 4–8, columns 6–8) (Szirtes, 2007; p. 175). The first 3 rows make up the dimensional matrix and include the exponents for each dimension (m, s, kg) of every influencing factor (see Table 1). The bottom rows include the exponents of each influencing factor that make up the individual dimensionless variables, denoted by  $\pi_1 \dots \pi_5$ .

	$D$	$w_e$	$w_p$	$\rho_g$	$\mu_g$	$d_p$	$\rho_p - \rho_g$	$g$
m	2	1	1	-3	-1	1	-3	1
s	-1	-1	-1	0	-1	0	0	-2
kg	0	0	0	1	1	0	1	0
$\pi_1$	1	0	0	0	0	-1.5	0	-0.5
$\pi_2$	0	1	0	0	0	-0.5	0	-0.5
$\pi_3$	0	0	1	0	0	-0.5	0	-0.5
$\pi_4$	0	0	0	1	0	0	-1	0
$\pi_5$	0	0	0	0	1	-1.5	-1	-0.5

$$\begin{aligned}
\pi_1 &= \frac{D}{\sqrt{d_p^3 g}} \\
\pi_2 &= \frac{w_e}{\sqrt{d_p g}} \\
\pi_3 &= \frac{w_p}{\sqrt{d_p g}} \\
\pi_4 &= \frac{\rho_g}{\rho_p - \rho_g} \\
\pi_5 &= \frac{\mu_g}{(\rho_p - \rho_g) \sqrt{d_p^3 g}}
\end{aligned} \tag{17}$$

Assuming a monomial form of the function  $\pi_1 = f(\pi_2, \pi_3, \pi_4, \pi_5)$  appears reasonable and was also done by [Shi and Fan \(1984; p. 339\)](#):

$$\pi_1 = c \prod_{i=2}^5 \pi_i^{\varepsilon_i} \tag{18}$$

where the constant  $c$  and the exponents  $\varepsilon_2 \dots \varepsilon_5$  are determined through experiments (calibration). Basic heuristics yield the following conclusions:

- When  $w_e = 0$  (i.e., when the fluidization stops), the particle dispersion coefficient  $D$  becomes 0 as well as long as the exponent  $\varepsilon_2 > 0$ . This means that fluidization is a necessary condition for any particle movement, which is physically consistent with the proposed model.
- On the other hand, when  $w_p = 0$  (i.e., when there is no flow of particles), then the particle dispersion coefficient would either become 0 in the case of  $\varepsilon_3 > 0$  or approach infinity in the case of  $\varepsilon_3 < 0$ . Neither result would be physically consistent. A better approach is to assume that  $\pi_3$  appears in the form of  $(1 + \pi_3)^{\varepsilon_3}$  in [Eq. 18](#), meaning the particle velocity  $w_p$  modifies the “basic” particle dispersion coefficient  $D$  without a cross-flow of particles.

Therefore, the equation for the particle dispersion coefficient is

$$\pi_1 = c \pi_2^{\varepsilon_2} (1 + \pi_3)^{\varepsilon_3} \pi_4^{\varepsilon_4} \pi_5^{\varepsilon_5} \tag{19}$$

## 4. Methods

This section describes the methods used to test whether the proposed PDM can accurately describe the cross-flow of particles and the impact of pressurized zones (air cushions) on the bed level. The following steps were taken to test (validate) the PDM:

- First, the PDM needed to be calibrated, meaning appropriate values for the constant and exponents of [Eq. 19](#) for the particle dispersion coefficient needed to be found. This is a prerequisite for any practical use of the PDM. A test rig was therefore used to measure particle dispersion coefficients at various operating points and calculate the dimensionless variables listed in [Eq. 17](#). Then, a non-linear least squares method was used to determine values for the constant and exponents in [Eq. 19](#) that best fit the measurements.
- After calibrating the PDM, the PDM was used to predict the outcome of experiments on a fluidized bed with particle cross-flow and an air cushion control system. However, any such experiment had to be dynamic in nature, and an analytical solution of the differential equation describing the PDM ([Eq. 15](#)) was therefore not feasible. As such, dynamic simulations were used to predict the outcome of experiments.
- A test rig with an air cushion control system was used to conduct step response tests. In such a test, a control system’s setpoint (the controlled bed level in this case) is changed suddenly. This is a common test to investigate and characterize a control system’s behavior ([Keviczky et al., 2019b; pp. 45–46](#)).

The PDM was validated by comparing the outcome of the step response tests with the simulation model’s predictions using both quantitative and qualitative methods.

- For a quantitative comparison, the differences (residuals) between the experimental and simulated (predicted) bed levels during a step response test were investigated. The predictions are considered to match the measurements if the residuals are normally distributed and centered around 0 ([Fahrmeier et al., 2021; p. 25](#)), thus validating the PDM. Pearson’s chi-square test with a significance level of 5 % ([Rolke and Gongora, 2021; p. 1886](#)) was used to evaluate whether the residuals were normally distributed.
- For a qualitative comparison, the reciprocal influence between bed levels at different locations inside the fluidized bed was investigated. If the simulated bed levels (predictions) behave physically consistently and match the experimental results, the PDM is validated.

The two main tools used for validating the PDM are described in detail in the following sections. The test rig, which was used both for calibrating the PDM and the step response tests, is described in [Section 4.1](#), and the dynamic simulation model is described in [Section 4.2](#).

### 4.1. Test rig

#### 4.1.1. Design

To calibrate and validate the proposed PDM, a test rig was used whose original purpose was to be a pilot plant of a thermal energy storage system. It contained a fluidized bed heat exchanger (FBHE) used to transfer thermal energy to and from particles, which acted as the storage material. Only this FBHE is of interest in this study since the exact modes by which particles and fluidization gas were supplied to the FBHE are immaterial to the proposed PDM. A description of the rest of the test rig, including process flow diagrams, is included in the data repository ([Thanheiser and Haider, 2025](#)).

The FBHE’s layout and measurement scheme is shown in [Fig. 3](#).

The FBHE consisted of four chambers in total: one inlet chamber ([Fig. 3](#), left), one outlet chamber ([Fig. 3](#), right), and two chambers with an air cushion control valve ([Fig. 3](#), center). A screw conveyor fed particles at a specified flow rate into the inlet chamber on the left. Particles left the system again by flowing over a weir in the outlet chamber on the right, which was located at a distance  $h_{\text{weir}}$  of 461.5 mm to the distributor floor.

The FBHE contained two tube banks in series, one in each chamber with an air cushion control valve. Each tube bank consisted of a staggered array of tubes with helical fins. The first tube bank and its chamber ([Fig. 3](#), center left) were slightly larger than the second one (center right), resulting in about 1 m and 0.8 m long chambers. The inlet and outlet chambers were about 0.2 m long each and did not contain any heat exchanger tubes. Detailed properties of the tube banks, which were the result of the original design process of the thermal energy storage system, are available in the data repository ([Thanheiser and Haider, 2025](#)). During experiments in this study, the tube banks were used to heat the fluidized bed to a specified temperature. The tube banks used supercritical CO<sub>2</sub> as the heat transfer fluid (HTF).

The fluidized bed had a width and height of about 0.5 m each and contained SiO<sub>2</sub> particles (quartz sand) with a mean diameter of about 175 μm, a sphericity of 0.8, a bed voidage at minimum fluidization conditions of 0.45 and a density of 2650 kg/m<sup>3</sup> ([Greenwood and Earnshaw, 1997; p. 344](#)). Each of the chambers had its own air box to provide fluidization air, whose mass flows  $\dot{m}_{A1} \dots \dot{m}_{A4}$  were measured using orifice plates (not pictured in [Fig. 3](#)). A porous plate in each chamber distributed the fluidization air across its respective chamber.

Design drawings and photographs of the test rig as well as detailed particle properties, such as particle size distribution, are available in the data repository ([Thanheiser and Haider, 2025](#)).

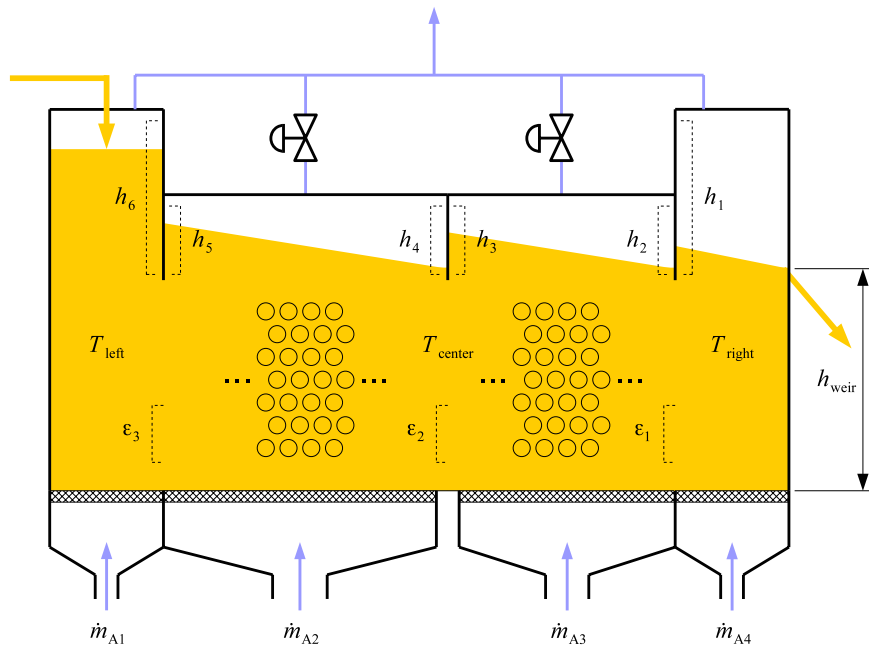


**Fig. 3.** Sketch of the FBHE and main variables. The orange area represents the fluidized bed, the checkered area the porous plate. Orange arrows represent particle flow. Blue arrows show flow of fluidization gas. Dotted lines indicate the position of pressure taps for bed level and voidage measurements. The circles in the center depict the heat exchanger tubes, whose axes are perpendicular to the particle flow direction. Measurements:  $h_1 \dots h_6$  bed levels,  $T$  bed temperatures,  $\epsilon_1 \dots \epsilon_3$  bed voidages,  $\dot{m}_{A1} \dots \dot{m}_{A4}$  fluidization gas mass flows,  $h_{weir}$  distance of outlet weir to distributor floor.

#### 4.1.2. Measurements

The bed level measurements  $h_1 \dots h_6$  shown in Fig. 3 were determined by measuring the quasi-hydrostatic pressures  $\Delta p$  close to the baffles that separated the chambers (see Eq. 10):

$$h = \frac{\Delta p}{\rho_p g (1 - \epsilon)} \quad (20)$$

The lower pressure taps were immersed in the fluidized bed while the upper pressure taps were located in the freeboard; see Fig. 3. The bed voidage  $\epsilon$  was again measured via the pressure difference within the bed:

$$\epsilon = 1 - \frac{\Delta p}{\rho_p g \Delta h} \quad (21)$$

In this case, the upper and lower pressure taps of  $\Delta p$  were both inside the fluidized bed at a vertical distance of  $\Delta h$ . Voidage was measured below each baffle separating the chambers,  $\epsilon_1 \dots \epsilon_3$  in Fig. 3, hence each bed level measurement had a voidage assigned.

The fictional bed density  $\Phi_{bed}$  was calculated from the measured bed level  $h$  and voidage  $\epsilon$  using Eq. 8. The particle dispersion coefficient  $D$  was calculated from a fictional density difference  $\Delta\Phi$  according to Eq. 5

$$D = -\dot{m}_s \frac{\Delta x}{\Delta\Phi} \quad (22)$$

where  $\Delta x$  is the distance between the points where the difference in fictional densities  $\Delta\Phi$  was measured and  $\dot{m}_s$  is the specific particle mass flow set as a boundary condition. All measurements of the particle dispersion coefficient  $D$  (which were only required for the calibration of the PDM) were conducted within the first chamber of the FBHE that had an air cushion valve (Fig. 3, center left). Hence,  $\Delta x$  was the horizontal distance between the measurements of  $h_4$  and  $h_5$  in Fig. 3, which was slightly smaller than the chamber's length of 1 m. Since all fictional densities within the same chamber experience identical air cushion pressures, the air cushion pressure was ignored in the calculation of the fictional density difference  $\Delta\Phi$  within the chamber:

$$\Delta\Phi = \Delta(\Phi_{bed} + \Phi_{AC}) = \Delta\Phi_{bed} \quad (23)$$

Therefore, only the bed's fictional densities  $\Phi_{bed}$  were measured to determine the particle dispersion coefficient  $D$ .

The temperature distribution in the bed was measured at three points: on the left in the inlet chamber  $T_{left}$ , in the center between the two tube banks  $T_{center}$ , and on the right in the outlet chamber  $T_{right}$ .

Data sheets of the measurement equipment used in the test rig and a detailed description of the calculations are available in the data repository (Thanheiser and Haider, 2025).

#### 4.1.3. Air cushion control system

A detailed or optimized design of the air cushion control system was not necessary to test the PDM and was therefore considered outside the scope of this work. Instead, a simple proportional-integral (PI) controller was chosen as the air cushion valves' controller. The control structure is shown in Fig. 4.

The FBHE had two air cushion valves controlling the bed levels in their respective chambers (Fig. 3), making the control system a multiple-input/multiple-output (MIMO) system. Each of the variables in Fig. 4 is therefore a  $1 \times 2$  array. The "plant" P in Fig. 4 is the mathematical representation of the FBHE and describes how changes in the air cushion control valves' actuating values (Y) affect the controlled bed levels (X). This is where the simulation model implemented the PDM. The PI-controller (C) controlled the air cushion valves (Y) to minimize the difference between the bed levels' setpoint (W) and their current values (X). The PI-controller had the following mathematical form:

$$Y = K_p \left( e(t) + \frac{1}{T_i} \int e(t) dt \right) \quad (24)$$

With  $K_p$  being the proportional gain and  $T_i$  the integration time. As

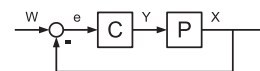


**Fig. 4.** Simplified control structure, consisting of the controller C and the plant P in a negative feedback loop. Variables: W bed level setpoints, X measured bed levels,  $e = W - X$  control error, Y air cushion valve actuating values (0%–100%).



mentioned above, determining these parameters for an optimal controller behavior was outside the scope of this work, so a proportional gain of  $K_p = 1\%/mm$  and an integration time of  $T_i = 10$  s were instead chosen based on practical experience. The simulation model was, however, used to investigate the control system's stability with the chosen controller parameters, as described in the data repository (Thanheiser and Haider, 2025).

A programmable logic controller (PLC) was used to control the entire test rig and to measure and record all system variables (measurements). It operated at a frequency of 10 Hz, which ensured the suppression of high-frequency disturbances in the measurements above the Nyquist frequency of 5 Hz while maintaining sufficiently fast reaction times.

#### 4.2. Dynamic simulations

A dynamic simulation model of the FBHE used the PDM to predict the outcome of experiments conducted with the test rig, thereby validating the PDM. The dynamic simulation tool Simulink was used to build the simulation model.

As shown in Fig. 3 and described in Section 4.1.1, a porous plate in each air box distributed fluidization air within its respective chamber. The simulation model took this distribution of fluidization air along the fluidized bed into account, which has been shown to have great influence on the quality of predictions (Farzaneh et al., 2013; p. 5803). Since the particle dispersion coefficient increases with increasing excess gas velocity (Sette et al., 2014; p. 77), a non-linear bed level gradient emerges when the fluidization is slightly uneven. The simulation model was able to predict the distribution of fluidization air across the porous plate distributor to accurately predict the bed levels at different specific particle flows.

As explained in Section 2, the baffles separating the individual chambers of the FBHE (see Fig. 3) restricted the movement of particles between them by blocking the particle splash created by bursting bubbles. Additionally, engineering and construction constraints led to a gap in the fluidization grid between the two chambers in the middle (60 mm wide), which is also pictured in Fig. 3. Both this gap and the baffles themselves resulted in a significantly larger resistance to particle flow in the baffles' vicinity. Additional resistance factors were added to the particle dispersion coefficient in the simulation model to account for this during simulations. Identifying the exact mode by which the baffles influenced the horizontal flow of particles was outside the scope of this work.

The simulation model used the same particles as in the test rig; see Section 4.1.1. Since the equation for the particle dispersion coefficient only considers the mean particle diameter an influencing factor (see Table 1), the simulation model effectively assumes particles of uniform size identical to the mean particle diameter in the test rig. By using the same minimum fluidization velocity in the simulation model as in the test rig, the simulation model also implicitly takes the particles' sphericity and bed voidage at minimum fluidization into account (Kunii and Levenspiel, 1991d; p. 69).

A detailed description of the simulation model, including discretization schemes of the differential equations and relevant boundary conditions, can be found in the data repository (Thanheiser and Haider, 2025); the simulation model itself is available in the software repository (Thanheiser, 2025).

#### 4.3. Experimental design

Measurements of the particle dispersion coefficient  $D$  to calibrate the PDM were conducted at various operating points of the test rig. The operating point parameters were chosen based on their expected influence on the particle dispersion coefficient  $D$  (see the dimensionless variables in Eq. 17) and are listed in Table 3.

Thus, by varying the parameters in Table 3, the impact of all dimensionless variables  $\pi_2 \dots \pi_5$  on the particle dispersion coefficient  $D$

**Table 3**

Operating point parameters for calibrating the PDM. Parameters:  $w_e/w_{mf}$  excess fluidization velocity relative to minimum fluidization velocity,  $\dot{m}_S$  specific particle mass flow,  $T_{bed}$  mean bed temperature.

Parameter	Values	Impact
$w_e/w_{mf}$	1.5	$\pi_2$
	2.1	
	2.7	
$\dot{m}_S$	4 kg/m <sup>2</sup> s	$\pi_3$
	5 kg/m <sup>2</sup> s	
	6 kg/m <sup>2</sup> s	
$T_{bed}$	55°C	$\pi_4$
	100°C	
	155°C	

(included in  $\pi_1$ ) were investigated. The design of experiments (DoE) included all possible combinations of these parameters (27).

The results of the calibration procedure largely informed the choice of operating points for the step response tests to validate the PDM (Table 4).

The parameter variations in Table 4 enabled clear observations of the air cushion system's dynamics and whether the PDM's predictions (simulations) were able to reproduce them.

All step response tests were conducted on the first chamber with an air cushion, with the controlled bed level on the downstream side of the chamber ( $h_4$ , see Fig. 3). After achieving a stationary state at a specified operating point, the control system's setpoint was changed instantaneously from  $h_4 = 515$  mm to  $h_4 = 485$  mm. Since the initial setpoint of  $h_4 = 515$  mm was too large to be attainable for the control system, the air cushion valve was fully open and the controller's output was saturated at 100 %, effectively disabling it. The valve only started to close after the step in the setpoint to  $h_4 = 485$  mm.

## 5. Results

### 5.1. Calibration

To calibrate the proposed PDM, measurements of the particle dispersion coefficient  $D$  were conducted on the test rig using the procedures described in Sections 4.1.2 and 4.3. In conjunction with other operating parameters (pressure and temperature), all dimensionless variables defined in Eq. 17 were then calculated.

A look at the responses of the dimensionless variables  $\pi_4$  and the inverse of  $\pi_5$  revealed that they were qualitatively very similar, as shown in Fig. 5.

It was therefore reasonable to assume that  $\pi_4$  and  $\pi_5$  only appear in combination with each other in Eq. 19, meaning that the exponents  $\varepsilon_4$  and  $\varepsilon_5$  are coupled. The Archimedes number  $Ar$  was chosen as such a combination (Kunii and Levenspiel, 1991d; p. 69):

$$Ar = \frac{\pi_4}{\pi_5^2} = \frac{d_p^3 \rho_g (\rho_p - \rho_g) g}{\mu_g^2} \quad (25)$$

Eq. 19 then reduces to

$$\pi_1 = c\pi_2^{\varepsilon_2} (1 + \pi_3)^{\varepsilon_3} Ar^{\varepsilon_{Ar}} \quad (26)$$

The practically identical responses of  $Ar$ ,  $\pi_4$ , and  $1/\pi_5$  shown in Fig. 5

**Table 4**

Operating point parameters for validating the PDM. See Table 3 for parameter descriptions.

Parameter	Values	Effect
$w_e/w_{mf}$	1.5	Slow bed level changes
	2.8	Fast bed level changes
$\dot{m}_S$	6 kg/m <sup>2</sup> s	Largest possible bed levels
$T_{bed}$	155°C	Largest possible bed levels

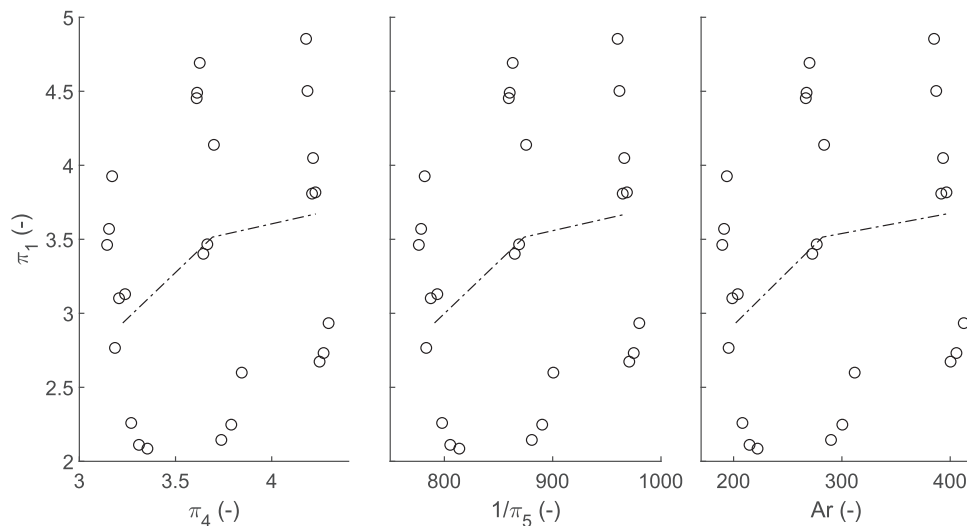


Fig. 5. Impact of  $\pi_4$ ,  $1/\pi_5$ , and the Archimedes number  $Ar$  on the dependent variable  $\pi_1$ . The dash-dotted lines describe mean values across different bed temperatures (see Table 3).

justify this approach. A non-linear least squares method was used to find the values of the constant  $c$  and the exponents  $\varepsilon_2$ ,  $\varepsilon_3$ , and  $\varepsilon_{Ar}$ , which are listed in Table 5.

The fit's adjusted  $R^2$  value, which describes how well the fit explains variations in the measurements adjusted for the number of regressors (Miles, 2005; pp. 1656–1657), is 0.966, indicating a good fit. Eq. 26 now reads with the included constant and exponents as

$$\pi_1 = 1.9318e4 \pi_2^{1.1017} (1 + \pi_3)^{-2.0494} Ar^{0.1086} \quad (27)$$

or directly as a function of the influencing factors for the particle dispersion coefficient  $D$  as

$$D = 1.9318e4 \sqrt{d_p^3 g} \left( \frac{w_e}{\sqrt{d_p g}} \right)^{1.1017} \left( 1 + \frac{w_p}{\sqrt{d_p g}} \right)^{-2.0494} \left( \frac{d_p^3 \rho_g (\rho_p - \rho_g) g}{\mu_g^2} \right)^{0.1086} \quad (28)$$

A variation of the excess fluidization velocity  $w_e$  has the greatest effect on the particle dispersion coefficient  $D$ , while variations of the particle flow  $w_p$  and the operating conditions represented by the Archimedes number  $Ar$  only slightly modify the particle dispersion coefficient  $D$ .

## 5.2. Validation

To validate the proposed PDM's ability to accurately represent the physical processes involved in an air cushion control system and predict its behavior, step response tests were conducted on the test rig as described in Section 4.3. The result of one of the tests is shown in Fig. 6.

Table 5

Fitted constant and exponents of Eq. 26.

Variable	Fitted value	Standard error	Rel. standard error
$c$	1.9318e4	3.9452e3	0.204
$\varepsilon_2$	1.1017	0.0476	0.043
$\varepsilon_3$	-2.0494	0.4853	-0.237
$\varepsilon_{Ar}$	0.1086	0.0371	0.342

Fig. 6 demonstrates how the measured bed level followed the one predicted by the proposed PDM very closely after suddenly decreasing the controller's setpoint from about 515 mm to 485 mm. The histogram of the probability distribution function (PDF) of the residuals (differences between measured and predicted values) is also shown in Fig. 6. The PDF was used for the quantitative method of validating the PDM as described in Section 4. The residuals' expected value  $\mu$  is very close to 0, and the p-value of Pearson's chi-square test  $p_\chi$  is greater than the 5 % level of significance. This indicates that the measurements followed the PDM's predictions and that all residuals were small random measurement errors normally distributed around the predictions. This confirms the PDM's ability to predict the bed level, thus validating the proposed

PDM.

As mentioned in Section 4, an additional qualitative method of comparison between the measurements and the PDM's predictions was used to validate the proposed PDM: whether the predicted reciprocal influence of bed levels during a step response test is physically consistent and compares well with the measurements. This comparison is demonstrated in Fig. 7.

As mentioned in Section 2 and 4.2, the baffles separating the chambers introduced an additional resistance to the flow of particles in their vicinity, which led to major discontinuities in the bed level between the zones (chambers); see the difference between  $h_5$  and  $h_6$  in Fig. 7. Therefore, the downstream bed levels  $h_1 \dots h_3$  could not be reasonably measured and only the upstream values  $h_5$ ,  $h_6$ , and the controlled level  $h_4$  (Fig. 7, small sketch) are shown in Fig. 7. The bed level  $h_5$ , which was upstream of  $h_4$  but in the same chamber, decreased by approximately the same amount as  $h_4$ . This is physically consistent as the air cushion pressure that pushed  $h_4$  down to a lower level acted on  $h_5$  in the same way.

However, the air cushion also impacted bed levels outside of its own chamber: the bed level  $h_6$  started to increase at the beginning of the step. Particles were still continuously carried into the first chamber, but the increase in air cushion pressure in the second chamber decreased the particle flow from the first into the second chamber. The particle flow

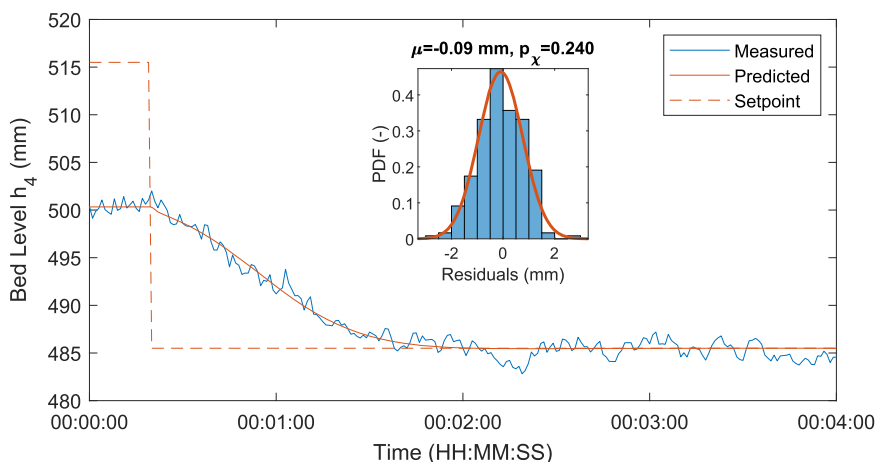


Fig. 6. Step response test, at  $w_e/w_{mf} = 2.8$ . Predicted (simulated) and measured bed level  $h_4$  after a step in the controller's setpoint from 515 mm to 485 mm.

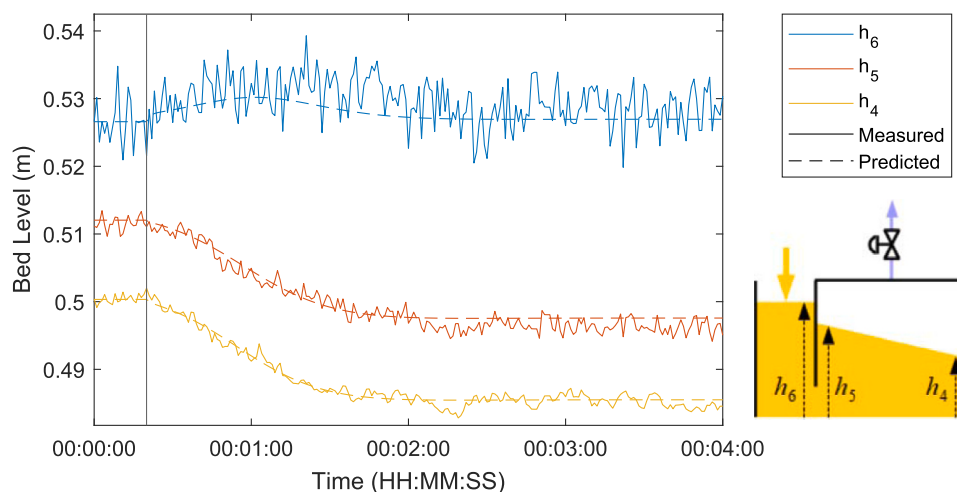


Fig. 7. Step response test. Upstream bed levels after a step from 515 mm to 485 mm at  $h_4$ . The black vertical line denotes the start of the step.

out of the first chamber was not reversed, only reduced, but since particles continued to be carried into the first chamber, the bed level there rose. After about one minute, when the bed levels  $h_5$  and  $h_4$  in the second chamber started to reach a stationary state again (when their second derivative with respect to time was zero), the bed level  $h_6$  started to decrease again. Once the system had reached a stationary state, the bed level  $h_6$  returned to its original value before the step response test.

Both results – the decrease in bed levels in the entire chamber where the air cushion increased its pressure and the temporarily increased bed level in the inlet chamber – are in line with a physically consistent behavior of the system, and the PDM was able to reproduce the measurements. This conclusively validates the proposed PDM.

Versions of Figs. 6 and 7 for all the other step response tests conducted are available in the data repository (Thanheiser and Haider, 2025). They all show largely the same results.

## 6. Discussion

Describing the processes involved in a fluidized bed with particle cross-flow whose bed levels are controlled by pressurized zones requires a new PDM. The results of the validation tests indicated that the proposed PDM is able to predict how different bed levels emerge due to the particle cross-flow and how the pressurized zones (air cushions) influence the bed levels.

The proposed PDM can be used to design and analyze air cushion

control systems, which are able to bring the bed levels of a fluidized bed as close to an immersed heat exchanger as possible to limit the number of particles bypassing it, thereby improving its efficiency. Although the air cushion control system used in the test rig in this study did not involve any sophisticated design, it proved effective during the step response tests. The bed levels reached a stationary state again in less than 2 minutes after the step, and the controller was able to hold the bed level within a few millimeters of the setpoint despite the oscillations in the measurements (Fig. 6).

The proposed PDM is still limited in terms of its general applicability.

- Not all influencing factors of particle dispersion could be investigated in this study. In particular, the fluidized bed's height and the configuration of the tube bank immersed in the fluidized bed were omitted since these factors could not be altered in the test rig used in this study. Future research should investigate these factors separately in dedicated test rigs, which will lead to additional dimensionless factors that will require the dimensional analysis to be repeated to obtain a more generalized equation for the particle dispersion coefficient.
- Although the particle diameter and particle density are already included in the model, their direct influence on particle dispersion could not be investigated since changing the particles in the test rig was not feasible. Future research should therefore include tests with different particle sizes and materials.

- Baffles that were used to separate individual pressurized zones in the fluidized bed introduced a greater resistance to particle flow than in the rest of the bed. As described in Section 2, this behavior was expected, but any detailed investigation was beyond the scope of this work. Accounting for the baffles' impact in the proposed PDM would enable the model to make global predictions of the bed level gradient along the entire fluidized bed and should therefore be a focus of future research.

Despite these limitations, the proposed PDM still provides a sound understanding of the physical processes involved in an air cushion control system, and its equation for the particle dispersion coefficient covers many important influencing factors. It therefore provides a solid basis for further improvements to the proposed PDM's general applicability, which can be achieved by investigating the impact of different bed heights, tube bank configurations, and particles, and modeling the impact of baffles on particle dispersion.

### 6.1. Comparison to other particle dispersion models

The novelty of the PDM developed in this work makes it difficult to compare to previously published models. The best source for a quantitative comparison of particle dispersion coefficients is the experimental results of Sette et al. (2014; p. 77), which Sette et al. recommended for use in their later fictional density model (Sette et al., 2015; p. 247). Their dispersion coefficients are about an order of magnitude lower than the dispersion coefficients observed in this work.

A qualitative comparison with other models reveals the following:

- In the proposed model, the particle dispersion coefficient increases with increasing excess fluidization velocity. This coincides with the results of other authors, such as Sette et al. (2014; p. 77), Shi and Fan (1984; p. 340), or Bellgardt and Werther (1986; p. 179).
- The particle dispersion coefficient slightly decreases with increasing particle flow in the proposed model. While Bellgardt and Werther found the dispersion coefficient to be independent of the particle flow rate (Bellgardt and Werther, 1986; p. 178), Shi and Fan's model predicts an increase in the dispersion coefficient with increasing lateral particle velocity (Shi and Fan, 1985; p. 27). Both models use tracer concentration gradients as the driving force of dispersion, which makes them difficult to compare to the model developed here. Since greater flows of particles lead to greater fictional density gradients, an increase in lateral mixing with increasing particle flow rates is already included in the fictional density gradient. The slight decrease in the dispersion coefficient with increasing flow rates suggests a greater flow resistance with increasing lateral particle velocity, which is comparable to a regular liquid experiencing a greater pressure loss at greater velocities when flowing through a pipe. Complete independence of the dispersion coefficient from the particle flow rate seems unlikely: the p-value (i.e., the probability that the measurements' pattern could have been obtained under the conditions of complete independence) (Greenland et al., 2016; p. 340) of  $\epsilon_3$  in Table 5 is about  $4.6e-4$ .
- The proposed model predicts a slight increase in the particle dispersion coefficient with increasing Archimedes numbers (see Eq. 28). An increase in the Archimedes number increases the minimum fluidization velocity (Kunii and Levenspiel, 1991d; pp. 68–70), and Kunii and Levenspiel agreed that an increase in the minimum fluidization velocity increases particle dispersion (Kunii and Levenspiel, 1991a; p. 222).

Thus, the results of the testing of the proposed PDM align well with past models.

### 6.2. Particle dispersion influencing factors

As mentioned in Section 3.2, the list of influencing factors of particle dispersion given in Table 1 is likely incomplete. Firstly, bed height at minimum fluidization conditions  $h_{mf}$  plays a role (Sette et al., 2014; p. 77), (Shi and Fan, 1984; p. 339), and thus the factor  $h_{mf}/d_p$  may be used as an additional dimensionless factor (Shi and Fan, 1984; p. 339) in the dimensional analysis.

Furthermore, as described in Section 2, an immersed tube bank impacts gross particle circulation and bubble dynamics, and its configuration therefore likely has a strong influence on particle dispersion. It also reduces the effective flow area for the horizontal particle flow, adding additional resistance to the horizontal dispersion of particles. The effective (vertical) cross-sections during the experiments presented in this work were between

$$0.64 \leq 1 - \frac{A_{\text{tubes}}}{A_0} \leq 0.67 \quad (29)$$

with  $A_{\text{tubes}}$  being the total cross-section of heat exchanger tubes (including fins) and  $A_0$  the flow area without any immersed bodies. Detailed geometric properties of the tube bank can be found in the data repository (Thanheiser and Haider, 2025). Since  $1 - A_{\text{tubes}}/A_0$  is a dimensionless number, it could be used directly as a pi-factor in the equation for the particle dispersion coefficient. However, the helical fins are likely to introduce an additional resistance beyond their obstruction of the flow area since the particles have to flow through the narrow gap between the fins, and a smaller fin pitch is known to obstruct particle flow (Jia, 2020; p. 312; Thanheiser et al., 2022; pp. 13–14). The tube's orientation may also play a role, with tubes parallel to the horizontal flow of particles leading to a different resistance than perpendicular tubes, even if the effective cross-section is identical. An in-line tube bank may also result in different resistances than a staggered array of tubes.

Since it was not possible to change the tube bank's configuration in the test rig nor the fluidized bed's height in a meaningful way, their influence could not be investigated in this work. The direct impact of the particle diameter, although included as an influencing factor, was not investigated either since all tests were conducted with the same particles. Any future development of the PDM should focus on these factors' influence on particle dispersion.

## 7. Conclusion

Detailed design and analysis of a control system that utilizes pressurized zones to control the bed level in a fluidized bed with particle cross-flow requires a mathematical model of the physical processes involved. In this study, a new dispersion model was developed that uses the concept of fictional densities to describe the flow of particles through the fluidized bed and its interaction with the pressurized zones, called air cushions. Dynamic simulations and experiments showed that the new dispersion model is able to accurately predict the outcome of step response tests of the air cushion control system, thereby validating the dispersion model.

The new particle dispersion model can be used to design sophisticated control structures of an air cushion control system, optimize its behavior, and analyze certain aspects of it such as control stability and robustness. Further research is required to achieve general applicability of the model, especially regarding the impacts of bed height, tube bank configuration, and baffles on particle dispersion.

### Role of the funding sources

The funders had no role in study design; in the collection, analysis, or interpretation of data; in the writing of the report; or in the decision to submit the article for publication.



## Funding

The information, data, or work presented in this paper was funded in part by the Advanced Research Projects Agency-Energy (ARPA-E), U.S. Department of Energy, under Award Number DE-AR0000996. The views and opinions of authors expressed herein do not necessarily state or reflect those of the United States Government or any agency thereof. The APC was funded by TU Wien Bibliothek.

## CRediT authorship contribution statement

**Thanheiser Stefan:** Writing – original draft, Visualization, Validation, Software, Methodology, Investigation, Formal analysis, Data curation, Conceptualization. **Haider Markus:** Writing – review & editing, Supervision, Resources, Project administration, Funding acquisition.

## Declaration of Competing Interest

The authors declare the following financial interests/personal relationships which may be considered as potential competing interests: Markus Haider has patents #WO2012027769A2, #WO2015172172A4, #WO2015188214A1, #WO2017210713A1, and #WO2020097657A1 issued to TU Wien (the authors' university), which encompass some technologies investigated in this work. Otherwise, the authors declare that they have no known competing financial interests or personal relationships that could have appeared to influence the work reported in this paper.

## Acknowledgments

Luke Magyar and Brett Bowan supported data collection; Timothy J. Held and Jason Miller supported with technical and scientific advice; Viktoria Illyes, Felix Birkelbach, and Florian Müller gave feedback on the manuscript. The authors acknowledge TU Wien Bibliothek for financial support through its Open Access Funding Program.

## Data availability

The data presented in this study is openly available in Zenodo at <https://doi.org/10.5281/zenodo.14833043>. Software for data analysis is openly available in Zenodo at <https://doi.org/10.5281/zenodo.14833128>.

## References

- Kunii, D., Levenspiel, O., 1991a. "The RTD and Size Distribution of Solids in Fluidized Beds," in *Fluidization Engineering*, 2nd ed. Butterworth-Heinemann, Boston, pp. 337–358. <https://doi.org/10.1016/B978-0-08-050664-7.50020-2>.
- Sette, E., Pallarès, D., Johnsson, F., 2015. Influence of bulk solids cross-flow on lateral mixing of fuel in dual fluidized beds (Dec.). *Fuel Process. Technol.* 140, 245–251. <https://doi.org/10.1016/j.fuproc.2015.09.017>.
- Daud, W.R.W., 2008. Fluidized bed dryers — recent advances (Apr.). *Adv. Powder Technol.* 19 (5), 403–418. [https://doi.org/10.1016/S0921-8831\(08\)60909-7](https://doi.org/10.1016/S0921-8831(08)60909-7).
- Gómez-Hernández, J., González-Gómez, P.A., Ni-Song, T., Briongos, J.V., Santana, D., 2018. Design of a solar linear particle receiver placed at the ground level (Nov.). *AIP Conf. Proc.* 2033 (1), 170005. <https://doi.org/10.1063/1.5067169>.
- Esence, T., Benoit, H., Poncin, D., Tessonneaud, M., Flamant, G., 2020. A shallow cross-flow fluidized-bed solar reactor for continuous calcination processes (Jan.). *Sol. Energy* 196, 389–398. <https://doi.org/10.1016/j.solener.2019.12.029>.
- Steiner, P., Schwaiger, K., Walter, H., Haider, M., 2016. Active Fluidized Bed Technology Used for Thermal Energy Storage (Jun.). *Proc. ASME 2016 10th Int. Conf. Energy Sustain.* Charlotte North Carol.: Am. Soc. Mech. Eng. Digit. Collect. <https://doi.org/10.1115/ES2016-59053>.
- Salatino, P., Ammendola, P., Bareschino, P., Chirone, R., Solimene, R., 2016. Improving the thermal performance of fluidized beds for concentrated solar power and thermal energy storage (Mar.). *Powder Technol.* 290, 97–101. <https://doi.org/10.1016/j.powtec.2015.07.036>.
- K.B. Schwaiger, "Development of a Novel Particle Reactor/Heat-Exchanger Technology for Thermal Energy Storages," PhD Thesis, TU Wien, Austria, 2016.
- Eder, C., Hofer, G., Pröll, T., 2021. Wall-to-bed heat transfer in bubbling fluidized bed reactors with an immersed heat exchanger and continuous particle exchange (May).

- Ind. Eng. Chem. Res.* 60 (19), 7417–7428. <https://doi.org/10.1021/acs.iecr.0c06331>.
- Keviczky, L., Bars, R., Hetthéssy, J., Bányász, C., 2019a. "Introduction," In: Keviczky, L., Bars, R., Hetthéssy, J., Bányász, C. (Eds.), *Control Engineering*. Springer, Singapore, pp. 1–36. [https://doi.org/10.1007/978-981-10-8297-9\\_1](https://doi.org/10.1007/978-981-10-8297-9_1).
- Thanheiser, S., Haider, M., 2025. Particle dispersion model dataset. Feb. 07 Zenodo. [doi: 10.5281/zenodo.14833043](https://doi.org/10.5281/zenodo.14833043).
- Thanheiser, S., 2025. Particle Dispersion Model Software. Feb. 07. Zenodo. <https://doi.org/10.5281/zenodo.14833128>.
- Kunii, D., Levenspiel, O., 1991a. "Solid Movement: Mixing, Segregation, and Staging," in *Fluidization Engineering*, 2nd ed. Butterworth-Heinemann, Boston, pp. 211–235. <https://doi.org/10.1016/B978-0-08-050664-7.50015-9>.
- Sette, E., Pallarès, D., Johnsson, F., 2014. Experimental evaluation of lateral mixing of bulk solids in a fluid-dynamically down-scaled bubbling fluidized bed (Sep.). *Powder Technol.* 263, 74–80. <https://doi.org/10.1016/j.powtec.2014.04.091>.
- Kunii, D., Levenspiel, O., 1991b. "Entrainment and Elutriation from Fluidized Beds," in *Fluidization Engineering*, 2nd ed. Butterworth-Heinemann, Boston, pp. 165–192. <https://doi.org/10.1016/B978-0-08-050664-7.50013-5>.
- Santana, D., Nauri, S., Acosta, A., García, N., Macías-Machín, A., 2005. Initial particle velocity spatial distribution from 2-D erupting bubbles in fluidized beds (Jan.). *Powder Technol.* 150 (1), 1–8. <https://doi.org/10.1016/j.powtec.2004.11.013>.
- Kunii, D., Levenspiel, O., 1969. Lateral dispersion of solid in fluidized beds. *J. Chem. Eng. 2* (1), 122–124. <https://doi.org/10.1252/cej.2.122>.
- Abanades, J.C., Grasa, G.S., 2001. Modeling the axial and lateral mixing of solids in fluidized beds (Nov.). *Ind. Eng. Chem. Res.* 40 (23), 5656–5665. <https://doi.org/10.1021/ie0009278>.
- Kunii, D., Levenspiel, O., 1991c. "Bubbling Fluidized Beds," in *Fluidization Engineering*, 2nd ed. Butterworth-Heinemann, Boston, pp. 137–164. <https://doi.org/10.1016/B978-0-08-050664-7.50012-3>.
- Pallarès, D., Díez, P., Johnsson, F., 2007. Experimental analysis of fuel mixing patterns in a fluidized bed (May). 12th Int. Conf. Fluid. - N. Horiz. *Fluid. Eng.* 929–936 (May).
- Olsson, J., Pallarès, D., Johnsson, F., 2012. Lateral fuel dispersion in a large-scale bubbling fluidized bed (May). *Chem. Eng. Sci.* 74, 148–159. <https://doi.org/10.1016/j.ces.2012.02.027>.
- Subbarao, D., Moghaddam, E., Bannard, J.E., 1985. Lateral mixing of particles in fluidized beds. *Chem. Eng. Sci.* 40 (10), 1988–1990. [https://doi.org/10.1016/0009-2509\(85\)80142-1](https://doi.org/10.1016/0009-2509(85)80142-1).
- M.M. Chen, B.T. Chao, and J. Liljegren, "The Effects of Bed Internals on the Solids Velocity Distribution in Gas Fluidized Beds," in *Proceedings of the Fourth International Conference on Fluidization*, D. Kunii and R. Toei, Eds., Kashikojima, Japan, May 1983, pp. 203–210.
- Asegehegn, T.W., Schreiber, M., Krautz, H.J., 2011a. Numerical simulation and experimental validation of bubble behavior in 2D gas–solid fluidized beds with immersed horizontal tubes (Nov.). *Chem. Eng. Sci.* 66 (21), 5410–5427. <https://doi.org/10.1016/j.ces.2011.07.056>.
- Li, T., Dietiker, J.-F., Zhang, Y., Shahnam, M., 2011. Cartesian grid simulations of bubbling fluidized beds with a horizontal tube bundle (Dec.). *Chem. Eng. Sci.* 66 (23), 6220–6231. <https://doi.org/10.1016/j.ces.2011.08.056>.
- Asegehegn, T.W., Schreiber, M., Krautz, H.J., 2011b. Investigation of bubble behavior in fluidized beds with and without immersed horizontal tubes using a digital image analysis technique (Jul.). *Powder Technol.* 210 (3), 248–260. <https://doi.org/10.1016/j.powtec.2011.03.025>.
- Kuipers, J. A. M., Prins, W., Van Swaaij, W.P.M., 1992. Numerical calculation of wall-to-bed heat-transfer coefficients in gas-fluidized beds (Jul.). *AIChE J.* 38 (7), 1079–1091. <https://doi.org/10.1002/aic.690380711>.
- Sette, E., Berdugo Vilches, T., Pallarès, D., Johnsson, F., 2016. Measuring fuel mixing under industrial fluidized-bed conditions – a camera-probe based fuel tracking system (Feb.). *Appl. Energy* 163, 304–312. <https://doi.org/10.1016/j.apenergy.2015.11.024>.
- Martínez Castilla, G., Larsson, A., Lundberg, L., Johnsson, F., Pallarès, D., 2020. A novel experimental method for determining lateral mixing of solids in fluidized beds – Quantification of the splash-zone contribution (Jun.). *Powder Technol.* 370, 96–103. <https://doi.org/10.1016/j.powtec.2020.05.036>.
- Shi, Y.-F., Fan, L.T., 1985. Lateral mixing of solids in gas–solid fluidized beds with continuous flow of solids (Jan.). *Powder Technol.* 41 (1), 23–28. [https://doi.org/10.1016/0032-5910\(85\)85070-1](https://doi.org/10.1016/0032-5910(85)85070-1).
- Bellgardt, D., Werther, J., 1986. A novel method for the investigation of particle mixing in gas-solid systems (Oct.). *Powder Technol.* 48 (2), 173–180. [https://doi.org/10.1016/0032-5910\(86\)80076-6](https://doi.org/10.1016/0032-5910(86)80076-6).
- Shi, Y.F., Fan, L.T., 1984. Lateral mixing of solids in batch gas-solids fluidized beds (Apr.). *Ind. Eng. Chem. Process Des. Dev.* 23 (2), 337–341. <https://doi.org/10.1021/i200025a026>.
- Einstein, A., 1905. Über die von der molekularkinetischen Theorie der Wärme geforderte Bewegung von in ruhenden Flüssigkeiten suspendierten Teilchen (May). *Ann. Phys.* 322 (8), 549–560. <https://doi.org/10.1002/andp.19053220806>.
- Köhler, A., Cano-Pleite, E., Soria-Verdugo, A., Pallarès, D., Johnsson, F., 2021. Modeling the motion of fuel particles in a fluidized bed (Dec.). *Fuel* 305, 121424. <https://doi.org/10.1016/j.fuel.2021.121424>.
- Liu, D., Chen, X., 2010. Lateral solids dispersion coefficient in large-scale fluidized beds (Nov.). *Combust. Flame* 157 (11), 2116–2124. <https://doi.org/10.1016/j.combustflame.2010.04.020>.
- Szirtes, T., 2007. "Systematic Determination of Complete Set of Products of Variables," In: Szirtes, T., Rózsa, P. (Eds.), in *Applied Dimensional Analysis and Modeling*, 2nd ed. Butterworth-Heinemann, Burlington, pp. 163–179. <https://doi.org/10.1016/B978-012370620-1.50014-9>.

- Kunii, D., Levenspiel, O., 1991d. "Fluidization and Mapping of Regimes," in *Fluidization Engineering*, 2nd ed. Butterworth-Heinemann, Boston, pp. 61–94. <https://doi.org/10.1016/B978-0-08-050664-7.50009-3>.
- Mori, S., Wen, C.Y., 1975. Estimation of bubble diameter in gaseous fluidized beds (Jan.). *AIChE J.* 21 (1), 109–115. <https://doi.org/10.1002/aic.690210114>.
- Oke, O., Lettieri, P., Salatino, P., Solimene, R., Mazzei, L., 2014. Numerical simulations of lateral solid mixing in gas-fluidized beds (Dec.). *Chem. Eng. Sci.* 120, 117–129. <https://doi.org/10.1016/j.ces.2014.08.049>.
- Farzaneh, M., Sasic, S., Almstedt, A.-E., Johnsson, F., Pallarès, D., 2013. A study of fuel particle movement in fluidized beds (Apr.). *Ind. Eng. Chem. Res.* 52 (16), 5791–5805. <https://doi.org/10.1021/ie301515v>.
- Guío-Pérez, D.C., Johnsson, F., Pallarès, D., 2023. Experimental investigation of the lateral mixing of large and light particles immersed in a fluidized bed (Aug.). *Fuel* 346, 128343. <https://doi.org/10.1016/j.fuel.2023.128343>.
- Salatino, P., Solimene, R., 2017. Mixing and segregation in fluidized bed thermochemical conversion of biomass (Jul.). *Powder Technol.* 316, 29–40. <https://doi.org/10.1016/j.powtec.2016.11.058>.
- Lundberg, L., Soria-Verdugo, A., Pallarès, D., Johansson, R., Thunman, H., 2017. The role of fuel mixing on char conversion in a fluidized bed (Jul.). *Powder Technol.* 316, 677–686. <https://doi.org/10.1016/j.powtec.2016.10.060>.
- Ferziger, J.H., Perić, M., Street, R.L., 2020. "Basic Concepts of Fluid Flow," in *Computational Methods for Fluid Dynamics*, 4th ed. Springer, Cham, pp. 1–21. [https://doi.org/10.1007/978-3-319-99693-6\\_1](https://doi.org/10.1007/978-3-319-99693-6_1).
- Greenwood, N.N., Earnshaw, A., 1997. "Silicon," (Eds.). in *Chemistry of the Elements*, 2nd ed. Butterworth-Heinemann, Oxford, pp. 328–366. <https://doi.org/10.1016/B978-0-7506-3365-9.50015-8> (Eds.).
- Wagner, W., Kretzschmar, H.-J., Span, R., Krauss, R., 2010. "D2 Properties of Selected Important Pure Substances," in *VDI Heat Atlas*, 2nd ed., in VDI-Buch. Springer, Berlin, Heidelberg, pp. 153–300. [https://doi.org/10.1007/978-3-540-77877-6\\_11](https://doi.org/10.1007/978-3-540-77877-6_11).
- Keviczky, L., Bars, R., Hetthéssy, J., Bányász, C., 2019b. "Description of Continuous Linear Systems in the Time, Operator and Frequency Domain," In: Keviczky, L., Bars, R., Hetthéssy, J., Bányász, C. (Eds.), *Control Engineering*. Springer, Singapore, pp. 37–126. [https://doi.org/10.1007/978-981-10-8297-9\\_2](https://doi.org/10.1007/978-981-10-8297-9_2).
- Fahrmeir, L., Kneib, T., Lang, S., Marx, B.D., 2021. "Regression Models," in *Regression*, 2nd ed. Springer, Berlin, Heidelberg, pp. 23–84. [https://doi.org/10.1007/978-3-662-63882-8\\_2](https://doi.org/10.1007/978-3-662-63882-8_2).
- Rolke, W., Gongora, C.G., 2021. A chi-square goodness-of-fit test for continuous distributions against a known alternative (Sep.). *Comput. Stat.* 36 (3), 1885–1900. <https://doi.org/10.1007/s00180-020-00997-x>.
- Miles, J., 2005. "R-Squared, Adjusted R-Squared," in *Encyclopedia of Statistics in Behavioral Science*. John Wiley & Sons, pp. 1655–1657. <https://doi.org/10.1002/0470013192.bsa526>.
- Greenland, S., et al., 2016. Statistical tests, P values, confidence intervals, and power: a guide to misinterpretations (Apr.). *Eur. J. Epidemiol.* 31 (4), 337–350. <https://doi.org/10.1007/s10654-016-0149-3>.
- Jia, D.E., 2020. "Heat and Mass Transfer," In: Grace, J., Bi, X., Ellis, N. (Eds.), in *Essentials of Fluidization Technology*. John Wiley & Sons, pp. 291–331. <https://doi.org/10.1002/9783527699483.ch14>.
- Thanheiser, S., Haider, M., Schwarzmayr, P., 2022. Experimental investigation of the heat transfer between finned tubes and a bubbling fluidized bed with horizontal sand mass flow. Art. no. 4, Feb. *Energies* 15 (4). <https://doi.org/10.3390/en15041316>.